Journal of the Brazilian Society of Mechanical Sciences and Engineering (2024) 46:36
https://doi.org/10.1007/s40430-023-04608-w

TECHNICAL PAPER

Dynamic curvature of a steel catenary riser on elastic seabed considering trench shoulder effects: an analytical model

Rahim Shoghi[1] · **Hodjat Shiri**[1] · **Celso Pupo Pesce**[2]

Received: 9 May 2023 / Accepted: 18 November 2023 / Published online: 16 December 2023

Abstract
Prediction of the fatigue life of steel catenary risers (SCR) in the touchdown zone is a challenging engineering design aspect of these popular elements. It is publically accepted that the gradual trench formation underneath the SCR due to cyclic oscillations may affect the fatigue life of the riser. However, due to the complex nature of the several mechanisms involving three different domains of the riser, seabed soil, and seawater, there is still no strong agreement on the beneficial or detrimental effects of the trench on the riser fatigue. Seabed soil stiffness and trench geometry play crucial roles in the accumulation of fatigue damage in the touchdown zone. There are several studies about the effect of seabed soil stiffness on fatigue. However, recent studies have proven the significance of trench geometry and identified the touchdown point oscillation amplitude as a key factor. In this study, a boundary layer solution was adapted to obtain the dynamic curvature oscillation of the riser in the touchdown zone on different areas of seabed trenches with a range of seabed stiffness. The proposed analytical model was validated against advanced finite element analysis using a commercial software. A range of seabed stiffness was examined, and the corresponding fatigue responses were compared. It was observed that in the elastic seabed, the effect of soil stiffness is attributed to the curvature oscillation amplitude and to the minimum local dynamic curvature that SCR can take in the touchdown zone. The proposed analytical model was found to be a simple and reliable tool for riser configuration studies with trench effects, particularly at the early stages of riser engineering design practice.

Keywords Steel catenary risers · Boundary layer method · Curvature dynamics · Fatigue response · Trench shoulder effect · Elastic soil

1 Introduction

Steel catenary risers (SCRs) are made of thin-wall steel pipes suspended from floating facilities to the seabed, in the form of a catenary. These attractive elements are common in offshore field developments for transferring gas and oil from the seabed to the floating systems or to convey water for some operational tasks. SCRs are subjected to cyclic and dynamic loads and are vulnerable to fatigue damage. Subsea surveys have shown that a trench is developed beneath the riser within a few years after installation [1], (see Fig. 1).

It is publically accepted that trench formation affects the fatigue life of the SCR in the touchdown zone (TDZ). However, there is still no coherent agreement on beneficial [2–4], or detrimental effects of the trench to fatigue damage [5–7]. The seabed soil stiffness and trench geometry have been identified as key influential factors in the accumulation of fatigue damage in the TDZ. The effect of seabed soil stiffness on fatigue has been widely investigated, showing that fatigue life is improved in softer seabed soils [4, 8–11]. However, recent studies have further focused on the significance of trench geometry and identified the touchdown point (TDP) oscillation amplitude as a key factor [3, 4, 12, 13]. As a matter of fact, in the simpler case of horizontal and flat (rigid or linear elastic) seabeds, the TDP excursion had already been shown to be a major contributor to fatigue damage [14–17]. Indeed, the TDP, a point that separates the

Technical Editor: Celso Kazuyuki Morooka.

✉ Hodjat Shiri
hshiri@mun.ca

[1] Civil Engineering Department, Faculty of Engineering and Applied Science, Memorial University of Newfoundland, St. John's, NL A1B 3X5, Canada

[2] Mechanical Engineering Department, Offshore Mechanics Laboratory, Escola Politecnica, University of São Paulo, São Paulo 05508-900, Brazil

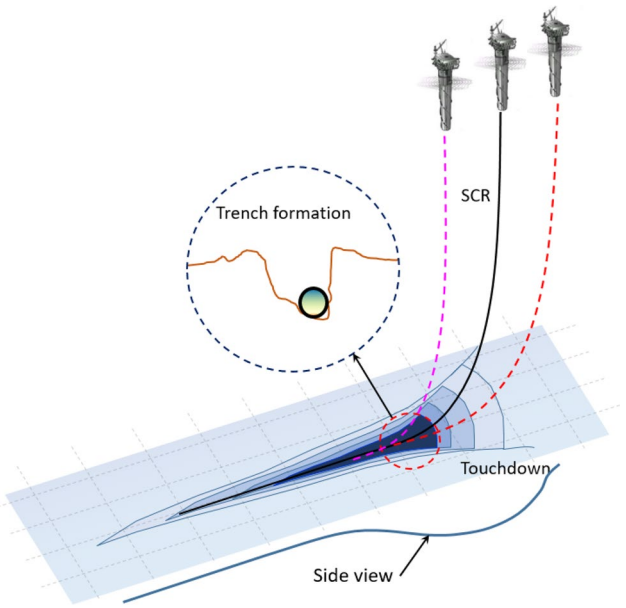

Fig. 1 Schematic view of trench formation under SCR in the touchdown zone

suspended from the supported part, i.e., a point of first contact (usually of tangency) with the soil, is, strictly speaking, a non-material one. Such a non-material point moves along the riser according to the motion of the structure, making the curvature at a given section to vary by large amounts as the pipe is, cyclically, suspended from and laid back on the soil. On the other hand, the soil stiffness governs the contact pressure between the riser and seabed; the contact pressure affects the magnitude of the shear force, which, in turn, is the gradient of the bending moment. As well-known, bending moment has a direct relation with riser curvature. The oscillation of the bending moment is, by far, the main contributor to the occurrence of cyclic normal stress fields in TDZ, so a major factor for fatigue damage, as tension is usually low in this region.

Currently, there are advanced nonlinear hysteretic (plastic) riser-seabed interaction models (e.g., Randolph and Quiggin [18]) that are built into the library of commercial software such as OrcaFlex®. These models are able to capture the cyclic seabed soil stiffness degradation and gradual trench formation along with the suction mobilization effect. However, there is a range of uncertainties in determining the input parameters of these models that makes them costly and less attractive in the industry, where the linear elastic seabed is still dominantly preferred because of simplicity, certainty, and acceptable accuracy. On the other hand, in the context of trench geometry, there is almost no difference between the key features of the trench profile created by using plastic riser-seabed interaction models and simple linear elastic seabed. The recent studies have further revealed the significance of the trench geometry compared with cyclic seabed stiffness degradation [12, 13]. In addition, the impact of the trench on fatigue life becomes more significant when the low-frequency vessel excursion is simulated. This, in turn, shows that assuming an elastic seabed with proper soil stiffness would not scarify the accuracy of soil simplification in terms of trench impact on fatigue. Therefore, the industry is looking for some simplified solutions preferably on the elastic seabed to incorporate the effect of nonlinear hysteretic riser-seabed interaction and trench formation in fatigue analysis. This, in turn, needs a deep understanding of the fundamental mechanisms occurring in a riser-seabed interaction process.

In this study, a comprehensive investigation was conducted to examine the significance of seabed geometry in dynamic fatigue damage accumulation of SCR in the TDZ. The study aimed to assess how the peak of the accumulated damage curve shifts from the mean TDP position, depending on the slope and stiffness of the seabed soil. This main objective was achieved by expanding the work conducted in [17, 19]. The dynamic equilibrium equations of a riser in the vertical plane was derived and matched to the dynamic equation of a tensioned Euler–Bernoulli beam supported on a linear elastic seabed, producing a local boundary layer solution, in TDZ, for the curvature oscillation of the riser, within a large range of seabed stiffness. For that, a sloped seabed was considered as a simplified, however proper, representation of the trench shoulders. A series of finite element analyses (FEA) was conducted to validate the analytical model. It was observed that the effect of soil stiffness is attributed to the dynamic curvature oscillation amplitude and to the minimum local curvature that SCR can take in the touchdown zone. The study further revealed the significance of trench geometry and showed that the seabed stiffness effect could also be assessed from a trench geometry perspective.

2 Boundary layer solution in TDZ

The dynamics of catenary-like structures has been widely investigated in the literature [20–23]. The planar problem of a SCR with the absence of shock against the soil, called as the subcritical dynamic regime, was investigated using the boundary layer method [14]. The authors obtained the dynamic curvature as a function of the time histories of tension and TDP displacement. Further qualitative and quantitative assessments were conducted in [17, 24, 25], by developing analytical solutions for the dynamic curvature of a SCR near the TDP. However, those studies were limited to the horizontal seabed, while the trench shoulders are sloped. In the current study, a local analytical quasi-static solution to the governing dynamic equilibrium equation for the suspended part of the riser is reassessed and matched to

a general quasi-static solution for the governing equation of a tensioned Euler–Bernoulli beam supported on a linear elastic sloped seabed. Different sloped seabeds, including those of 'negative' slopes (corresponding to the far vessel offset zone, FOZ) and positive slopes (corresponding to the near vessel offset zone, NOZ), are considered (see Fig. 2).

When the vessel moves away from the riser (far offset), the TDP oscillates on the negative shoulder of the trench (FOZ). Likewise, when the vessel moves toward the SCR (near offset), the TDP oscillates on the positive shoulder of the trench (NOZ). Following Aranha et al. [14] and Pesce et al. [16], the effects of the vessel motions due to incoming sea waves are modeled through the corresponding variations in tension and in the TDP oscillations in the TDZ. In order to obtain the riser-seabed interaction, first, the dynamic curvatures of the suspended and supported sections are formulated and, then, the results are matched at the TDP.

2.1 Planar dynamic equations for the suspended part of the SCR

Figure 3 shows the schematic riser dynamics around the static configuration. Only the planar problem is herein addressed. Small strains and linear constitutive equations are assumed throughout the whole derivation.

As worked out in the Appendix, based on Pesce [15], let the planar static equilibrium configuration be expressed by three functions: $\theta(s)$, the angle of the center line of the SCR with respect to the horizontal and the fields $Q(s)$ and $T(s)$, the static shear force and effective tension, respectively, resulting from the immersed weight per unit length, q, and from the static component of the hydrodynamic loading. The curvilinear arch length coordinate s is measured from a static reference position taken as the TDP of a homologous cable problem. It is worth noting that the hydrodynamic load depends on the geometric configuration, which turns the procedure of finding the static equilibrium configuration a highly nonlinear problem that has to be solved iteratively, in advance.

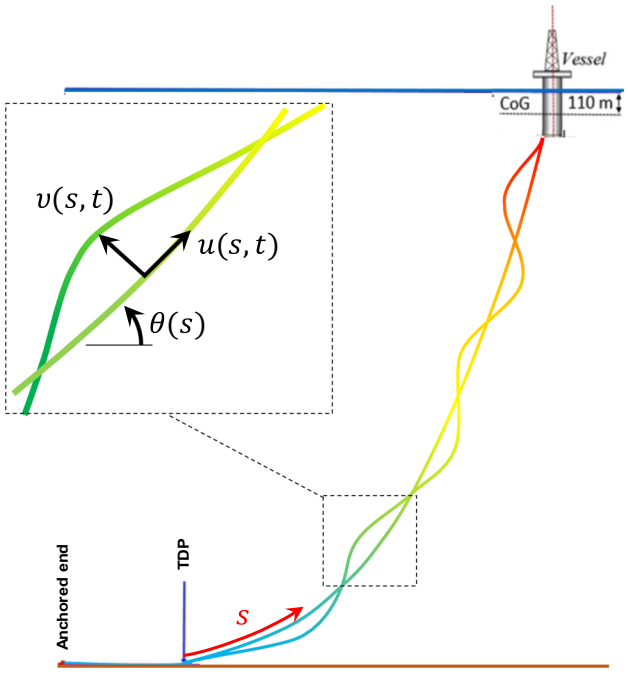

Fig. 3 Schematic view of SCR configuration

The planar kinematics is defined around the supposedly known static equilibrium configuration (see Fig. 4). The displacement fields $u(s,t)$ and $v(s,t)$ are considered small and in the tangential and normal directions of the center line of the SCR.

The partial differential equations governing the dynamics of the riser around the static equilibrium configuration and projected onto the tangential and normal directions may then be written in the following form [see Appendix, Eq. (42)]:

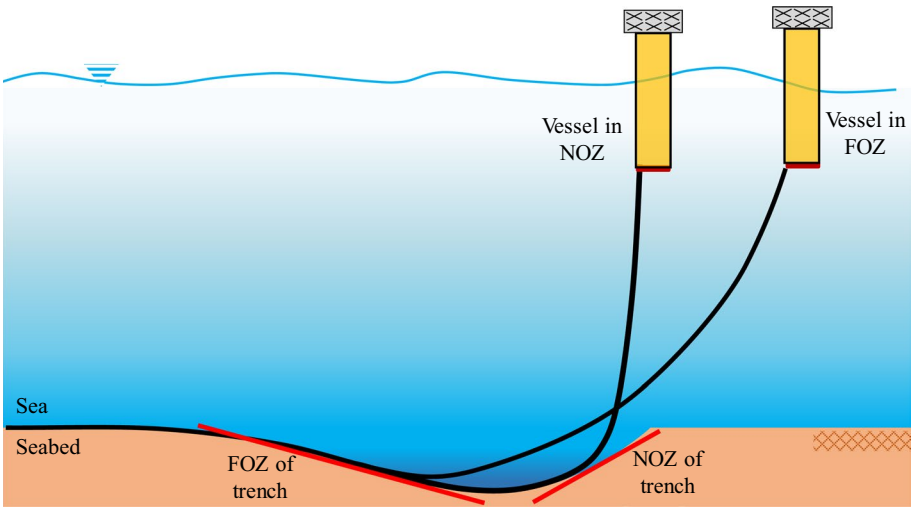

Fig. 2 Schematic view of trench and vessel configuration

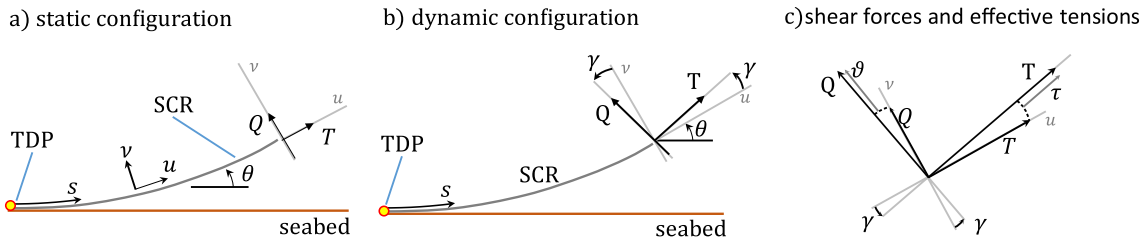

Fig. 4 Static and dynamic configuration of SCR in the TDZ

$$\begin{aligned}
&\frac{\partial T}{\partial s} - (T\gamma + Q)\frac{\mathrm{d}\theta}{\mathrm{d}s} - \frac{\partial}{\partial s}(Q\gamma) + h_u + \varpi_u - q\sin\theta = m\frac{\partial^2 u}{\partial t^2}\\
&\frac{\partial Q}{\partial s} + (T - Q\gamma)\frac{\mathrm{d}\theta}{\mathrm{d}s} + \frac{\partial}{\partial s}(T\gamma) + h_v + \varpi_v - q\cos\theta = m\frac{\partial^2 v}{\partial t^2}
\end{aligned} \tag{1}$$

in Eq. (1),

$$\begin{aligned}
\Theta(s,t) &= \theta(s) + \gamma(s,t)\\
T(s,t) &= T(s) + \tau(s,t)\\
Q(s,t) &= Q(s) + \vartheta(s,t)
\end{aligned} \tag{2}$$

are, respectively, the instantaneous angle of the line with the horizontal, the total effective tension and the shear force, being $\gamma(s,t)$, $\tau(s,t)$ and $\vartheta(s,t)$ their corresponding perturbed quantities around the static configuration, resulting from dynamic loads acting on the riser in the vertical plane. The terms $h_{u,v}(s)$ and $\varpi_{u,v}(s,t)$ are the components of the static and dynamic parcels of the hydrodynamic force, in the tangential and normal direction, respectively. The last ones are due to the relative external water flow with respect to the riser, at section s, usually modeled through the well-known Morison's formula.

To first order, the following well-known linear kinematic relation is supposed valid, Eq. (37):

$$\gamma(s,t) = \frac{\partial v}{\partial s} + u\frac{\mathrm{d}\theta}{\mathrm{d}s} \tag{3}$$

and Eq. (1) may be alternatively written, Eq. (43):

$$\begin{aligned}
&\frac{\partial T}{\partial s} - \left[T\left(\frac{\partial v}{\partial s} + u\frac{\mathrm{d}\theta}{\mathrm{d}s}\right) + Q\right]\frac{\mathrm{d}\theta}{\mathrm{d}s} - \frac{\partial}{\partial s}\left[Q\left(\frac{\partial v}{\partial s} + u\frac{\mathrm{d}\theta}{\mathrm{d}s}\right)\right]\\
&\quad + h_u + \varpi_u - q\sin\theta = m\frac{\partial^2 u}{\partial t^2}\\
&\frac{\partial Q}{\partial s} + \left[T - Q\left(\frac{\partial v}{\partial s} + u\frac{\mathrm{d}\theta}{\mathrm{d}s}\right)\right]\frac{\mathrm{d}\theta}{\mathrm{d}s} + \frac{\partial}{\partial s}\left[T\left(\frac{\partial v}{\partial s} + u\frac{\mathrm{d}\theta}{\mathrm{d}s}\right)\right]\\
&\quad + h_v + \varpi_v - q\cos\theta = m\frac{\partial^2 v}{\partial t^2}
\end{aligned} \tag{4}$$

Notice, in Eqs. (1) and (4), the coupling between the displacement field arises from the static curvature. These equations should be integrated numerically, for given boundary and initial conditions, to solve for the displacements $u(s,t)$ and $v(s,t)$ around the static configuration.

On the other hand, considering that no external distributed moment is applied to the line and consistently disregarding the effects of rotatory inertia due to the slenderness of the structure and by using the usual Kirchhoff–Love hypotheses [26], the following constitutive equation may be assumed valid, Eq. (51):

$$M(s,t) = EI\frac{\partial\Theta}{\partial s} = EI\chi(s,t) \tag{5}$$

where M(s,t) is the bending moment, EI is the bending stiffness at section s, and $\chi(s,t)$ is the total curvature. Then, Eq. (1b) that governs the normal displacement, $v(s,t)$, may be put in the following form, with EI assumed a constant value along s [Eq. (55)]:

$$-EI\frac{\partial^2\chi}{\partial s^2} - \gamma EI\frac{d\theta}{ds}\frac{\partial\chi}{\partial s} + T\chi + \gamma\frac{\partial T}{\partial s} + h_v + \varpi_v - q\cos\theta = m\frac{\partial^2 v}{\partial t^2} \tag{6}$$

Equation (6) governs the dynamics of the suspended part of the riser in the normal direction, around the static configuration. Notice that Eq. (1a) could be discussed further, regarding axial dynamics and respective time scales, what enables one to gauge the behavior of the dynamic tension along the riser. A thorough and detailed analysis may be found in Pesce [15], chapter 4, section 4.1, pages 191–203.

Close to TDP, it can be shown that with an error of order $\sim O\left(\chi_0\lambda\cdot\max\left\{\theta\gamma;\gamma^2;\theta^2\right\}\right)$, where $\chi_0 = q/T_0$ is the curvature at TDP for a cable on a flat and rigid seabed, include tension T_0 at TDP; and $\lambda = \sqrt{EI/T_0}$ is the length scale of the bending stiffness effect at TDP that Eq. (6) reduces to [14, 15, 25]:

$$-EI\frac{\partial^2\chi}{\partial s^2} + T\chi + \gamma\frac{\partial T}{\partial s} + h_v + \varpi_v - q \cong m\frac{\partial^2 v}{\partial t^2} \tag{7}$$

Moreover, considering in this vicinity that, to first order, $\gamma(s,t) \approx \partial v/\partial s$, Eq. (7) may be approximated in the form:

$$-\lambda^2\frac{\partial^2\chi}{\partial s^2} + \frac{1}{T_0}\left(T\chi + \frac{\partial v}{\partial s}\frac{\partial T}{\partial s} + h_v + \varpi_v^V\right) - \chi_0 \cong \frac{1}{c_0^2}\frac{\partial^2 v}{\partial t^2} \tag{8}$$

where $c_0 = \sqrt{T_0/(m+m_a)}$ is the transversal wave celerity of a tensioned cable, a reference velocity scale for the problem, with m_a the added mass per unit length. Notice that in Eq. (8), only the viscous hydrodynamic forces, $(h_v + \varpi_v^V)$, was left on the LHS, as the inertial parcel, proportional to the added mass and to the normal acceleration was brought to the RHS. It can be also shown that at TDP vicinity, the viscous hydrodynamic forces are locally of second order, hence not dominant governing terms [14, 15, 25].

Moreover, it can be also shown that $\partial\tau/\partial s(L/EA) \approx O\left[v_0(\omega/\omega_u)^2\right]$, where $\omega_u = (\pi/L)\sqrt{EA/m}$ is a frequency scale for the axial vibration of the riser considering a total suspended length L, $v_0 = u_0/L$ is the typical non-dimensional axial displacement amplitude, and EA is the axial stiffness [15]. For a typical 10″3/4 SCR in 1000 m water depth, this value is of order 10^{-5}. Also, from the catenary equation near TDP, the static effective tension may be approximated as $T(s) \approx T_0 \sec\theta(s) \cong T_0(1 + O(\theta^2))$, such that its derivative with respect to s may be written, $T'(s) \cong T_0 \tan\theta(s)\sec\theta(s)\chi_0 \cong T_0\chi_0\theta(s) = q\theta(s)$. Therefore, in this neighborhood, the total effective tension can be well-approximated by $T(s,t) \cong T_0 + \tau(0,t)$, and it is the only significant term that is left in the parenthesis of Eq. (8). Henceforth, the dynamic tension at TDP vicinity will be simply referred to as $\tau(0,t) = \tau(t)$. So, retaining only the dominant terms, Eq. (8) is written:

$$-\lambda^2\frac{\partial^2\chi}{\partial s^2} + \left(1 + \frac{\tau(t)}{T_0}\right)\chi - \chi_0 \cong \frac{1}{c_0^2}\frac{\partial^2 v}{\partial t^2} \tag{9}$$

Still, Eq. (9) is a dynamic equilibrium equation, since the inertial term appears explicitly in its RHS. However, as shown in Aranha et al. [14], and discussed further in Pesce et al. [25], and in great detail in Pesce [15], a quasi-static approximation to Eq. (9) may be constructed with an error of order $O(\mathcal{M}^2)$, where $\mathcal{M} = V_0/c_0$ is a non-dimensional number formed by the ratio between the typical speed of the TDP (a non-material point), V_0, and the transversal wave celerity of a cable, $c_0 = \sqrt{T_0/(m+m_a)}$. As a matter of fact, this number regulates the possible impact of a cable against the seabed. If $\mathcal{M} > 1$, i.e., if the TDP speed is larger than the cable transversal wave celerity, a shock will take place. Otherwise, if $\mathcal{M} < 1$, shock will not exist. It is like letting enough time to the cable to adjust its curvature, smoothly, at the tangency point (TDP) as it moves forward or backward. The first dynamic regime, $\mathcal{M} > 1$, is called supercritical. The second regime, $\mathcal{M} < 1$, is named subcritical. As pointed out in [15, 17], notice that $\mathcal{M} = V_0/c_0$ is physically analogous to the classic 'Mach' number in compressible flows. In the subcritical regime, the TDP can be viewed as an analogous of the instantaneous center of rotation of a 'variable radius rigid disk' that rolls back and forth and without slipping on a smooth surface [16].

This being said, it has been shown by Aranha et al. [14], and discussed further by Pesce [15] that the inertial term is of order:

$$\frac{\chi_0}{c_0^2}\frac{\partial^2 v}{\partial t^2} = O(\mathcal{M}^2) \tag{10}$$

Therefore, if a subcritical regime is assumed, such that $\mathcal{M}^2 \ll 1$, Eq. (9) may be written:

$$-\lambda^2\frac{\partial^2\chi}{\partial s^2} + \left(1 + \frac{\tau(t)}{T_0}\right)\chi = \chi_0(1 + O(\mathcal{M}^2)) \tag{11}$$

or, correct to $O(\mathcal{M}^2)$, in a purely *quasi-static* form as,

$$-\lambda^2\frac{\partial^2\chi}{\partial s^2} + \left(1 + \frac{\tau(t)}{T_0}\right)\chi = \chi_0 \tag{12}$$

Equation (12) governs the total curvature of the suspended part of the riser, in the TDP region, once a subcritical dynamic regime is assumed to take place. Hereinafter, the quasi-static solution for this equation will be simply referred to as the 'dynamic curvature' along the suspended part of the riser in the TDZ.

The general solution for Eq. (12) is given by (see [17]):

$$\begin{aligned}\chi(s,t) = &\frac{\chi_0}{1+f(t)} + c_1(t)\exp -\left(\sqrt{1+f(t)}\right)\left(s - s_K(t)\right)/\lambda \\ &+ c_2(t)\exp\sqrt{1+f(t)}\left(s - s_K(t)\right)/\lambda\end{aligned} \tag{13}$$

where $f(t) = \tau(t)/T_0$ is the non-dimensional dynamic tension at TDZ and $s_K(t)$ defines the still unknown actual TDP position, i.e., the instantaneous position of the point at which the riser touches the seabed. Assuming a finite solution in the far field, i.e., as $\left(s - s_K(t)\right)/\lambda \to \infty$, it follows that $c_2(t) = 0$. Also, Eq. (13) should encompass the seabed curvature, χ_{sb}, at TDP, so that $c_1(t) = \chi_{\text{sb}} - \chi_0/(1+f(t))$. Equation (13) can then be rewritten as the general 'dynamic curvature' of the suspended part of the riser in TDZ as follows:

$$\chi(s,t) = \frac{\chi_0}{1+f(t)} + \left(\chi_{\text{sb}} - \frac{\chi_0}{1+f(t)}\right)C_1(t)\exp\left(-\sqrt{1+f(t)}\left(s - s_K(t)\right)/\lambda\right) \tag{14}$$

Local non-dimensional variables in the form of $\xi = x/\lambda$ and $\eta(\xi,t) = y(s,t)/\lambda$ are used to define position and the elastic line quota, which x and y are horizontal and vertical axes of a Cartesian frame with origin at the TDP. Also, the non-dimensional curvature ($\eta'' = \lambda y'' \approx \lambda\chi$), related to bending moment, the third derivative (η'''), related to the shear force, and, by integration, the slope (η'), are then determined as:

$$\eta''(\xi,t)=\frac{\lambda\chi_0}{1+f(t)}+\lambda\left(\chi_{sb}-\frac{\chi_0}{1+f(t)}\right)C_1(t)\exp\left(-\sqrt{1+f(t)}(\xi-\xi_K(t))\right) \quad (15)$$

$$\eta'''(\xi,t)=-\sqrt{1+f(t)}\lambda\left(\chi_{sb}-\frac{\chi_0}{1+f(t)}\right)C_1(t)\exp\left(-\sqrt{1+f(t)}(\xi-\xi_K(t))\right) \quad (16)$$

$$\eta'(\xi,t)=\frac{\lambda\chi_0(\xi-\xi_0(t))}{1+f(t)}-\frac{\lambda}{\sqrt{1+f(t)}}\left(\chi_{sb}-\frac{\chi_0}{1+f(t)}\right)C_1(t)\exp\left(-\sqrt{1+f(t)}(\xi-\xi_K(t))\right) \quad (17)$$

where $\xi_0(t)=x_0(t)/\lambda$ is a known (usually assumed cyclic) function, to consider the TDP oscillation of a homologous cable case, used as a local driving term [17], e.g., $x_0(t)=a_0\cos\left(2\pi t/T_s+\varphi\right)$ being a_0 the cable case TDP oscillation amplitude and φ the phase, relative to the dynamic tension. Notice also that the non-dimensional boundary layer solution for the static problem is recovered through Eqs. (15)–(17) by taking $f(t)=0$ and $\xi_0(t)=0$.

Generally, the non-dimensional curvature solution for the suspended part in the TDZ can be expressed by substituting the still unknown function $\xi=\xi_K(t)$ in Eqs. (15)–(17), leading to:

$$\eta'(\xi_K,t)=\frac{\lambda\chi_0}{1+f(t)}\left(\xi_K(t)-\xi_0(t)-\frac{C_1(t)}{\sqrt{1+f(t)}}\right) \quad (18)$$

$$\eta''(\xi_K,t)=\frac{\lambda\chi_0}{1+f(t)}(1-C_1(t)) \quad (19)$$

$$\eta'''(\xi_K,t)=\frac{\lambda\chi_0}{\sqrt{1+f(t)}}C_1(t) \quad (20)$$

Equations (18)–(20) are dependent on two unknown functions of time, $\xi_K(t)$ and $C_1(t)$, which will be found by a classical matching procedure with an analytical solution for the part of the riser supported on the seabed. In other words, the non-dimensional TDP relocation will be found as a function of soil stiffness, seabed slope, and time.

2.2 Dynamic equations for the supported part of the SCR on the seabed

The planar problem of riser dynamics on elastic soil is herein solved assuming known the static tension at TDP, T_0 and the functions $\tau(t)$ and $x_0(t)$ as two dynamic driving terms. Let y be the vertical coordinate for the SCR center line, measured from a certain reference position. The still unknown actual TDP position (i.e., the point where the riser touches the seabed) has been defined as $s_K(t)$, such that $y(s_K(t))=y_{sb}(s_K(t))$. For a flat and horizontal seabed, this geometric condition is simply given by $y(s_K(t))=0$. For the part of the riser resting on the seabed, a non-separation restraining condition is assumed for $s<s_K(t)$. Taking a not too soft soil, the slope may be approximated by $\theta\approx \mathrm{d}y/\mathrm{d}x$, $s\approx x$, and the curvature by $\chi(s)\approx\chi(x)\approx \mathrm{d}^2y/\mathrm{d}x^2$. Then, assuming a linearly elastic seabed, the non-dimensional soil rigidity can be defined as follows:

$$K=\frac{kEI}{T_0^2}=\frac{k\lambda^2}{T_0}=\frac{k\lambda^4}{EI}=\chi_0\lambda\frac{k\lambda}{q} \quad (21)$$

In Eq. (21), k is the soil modulus. The quasi-static equation of an Euler–Bernoulli beam supported on a linear elastic soil, subjected to an applied dynamic tension, can be written in a non-dimensional form as follows, where the inertia term is disregarded for the subcritical regime with an error of order $(\lambda/L)^2$ (λ and L are boundary layer length and suspended riser length, respectively) [17]:

$$\frac{\partial^4\eta}{\partial\xi^4}-\left(1+\frac{\tau(t)}{T_0}\right)\frac{\partial^2\eta}{\partial\xi^2}+K\eta=K\eta_{sb};\quad \xi<\xi_K(t) \quad (22)$$

In Eq. (22), $\eta_{sb}=\xi\tan\theta_{sb}$ represents the seabed configuration, such that $\theta_{sb}=0$ for the flat and horizontal seabed, $\theta_{sb}>0$ for NOZ, and $\theta_{sb}<0$ for FOZ. The following far-field boundary conditions are assumed to hold: $\lim_{\xi\to-\infty}\eta(\xi)\cong\lim_{\xi\to-\infty}K\eta_{sb}$ and $\lim_{\xi\to\xi_K}\eta(\xi)\cong\eta_{sb}(\xi_K(t))$.

The solution of Eq. (22), and corresponding derivatives in space, can be written, for $\xi<\xi_K(t)$, i.e., for the part supported on the seabed, in the form of the following non-dimensional equations:

$$\eta(\xi,t)=C(t)\exp\left(\frac{K^{0.25}}{\sqrt{2}}(\xi-\xi_K(t))\right)\sin\left(\frac{K^{0.25}}{\sqrt{2}}(\xi-\xi_K(t))\right)+\xi\tan\theta_{sb} \quad (23)$$

$$\eta'(\xi,t)=\frac{K^{0.25}}{\sqrt{2}}C(t)\exp\left(\frac{K^{0.25}}{\sqrt{2}}(\xi-\xi_K(t))\right)\left\{\sin\left(\frac{K^{0.25}}{\sqrt{2}}(\xi-\xi_K(t))\right)+\cos\left(\frac{K^{0.25}}{\sqrt{2}}(\xi-\xi_K(t))\right)\right\}+\tan\theta_{sb} \quad (24)$$

$$\eta''(\xi,t)=K^{0.5}C(t)\exp\left(\frac{K^{0.25}}{\sqrt{2}}(\xi-\xi_K(t))\right)\cos\left(\frac{K^{0.25}}{\sqrt{2}}(\xi-\xi_K(t))\right) \quad (25)$$

$$\eta'''(\xi,t)=\frac{K^{0.75}}{\sqrt{2}}C(t)\exp\left(\frac{K^{0.25}}{\sqrt{2}}(\xi-\xi_K(t))\right)\left\{\cos\left(\frac{K^{0.25}}{\sqrt{2}}(\xi-\xi_K(t))\right)-\sin\left(\frac{K^{0.25}}{\sqrt{2}}(\xi-\xi_K(t))\right)\right\} \quad (26)$$

On the supported part, the values of the derivatives of the elastic line at the still unknown actual TDP (supposing the seabed represented locally by a constant slope) can be found by substituting $\xi=\xi_K(t)$ in Eqs. (24)–(26). Therefore,

$$\eta'\left(\xi_K,t\right)=\frac{K^{0.25}}{\sqrt{2}}C(t)+\tan\theta_{\mathrm{sb}} \tag{27}$$

$$\eta''(\xi,t)=K^{0.5}C(t) \tag{28}$$

$$\eta'''(\xi,t)=\frac{K^{0.75}}{\sqrt{2}}C(t) \tag{29}$$

Notice that a new unknown function of time, $C(t)$, appeared. Next, the above obtained solution, valid for the supported part will then be matched with the one valid for the suspended part to find the still unknown TDP relocation, as a function of soil stiffness, seabed slope, and time.

2.3 Matching solutions at TDP

Matching both sets of Eqs. (18)–(20) and (27)–(29) leads to a system of three linear algebraic equations, for the three unknowns, $\xi_K(t)$, $C_1(t)$ and $C(t)$:

$$\begin{cases}\frac{\lambda\chi_0}{1+f(t)}\left(\xi_K(t)-\xi_0(t)-\frac{C_1(t)}{\sqrt{1+f(t)}}\right)=\frac{K^{0.25}}{\sqrt{2}}C(t)+\tan\theta_{\mathrm{sb}}\\ \frac{\lambda\chi_0}{1+f(t)}\left(1-C_1(t)\right)=K^{0.5}C(t)\\ \frac{\lambda\chi_0}{\sqrt{1+f(t)}}C_1(t)=\frac{K^{0.75}}{\sqrt{2}}C(t)\end{cases} \tag{30}$$

The solution of Eq. (30) gives, as the main result, the non-dimensional ideal TDP relocation, $\xi_K(t)$, written as an explicit function of soil stiffness, seabed slope and of the two dynamic driving terms:

$$\xi_K(t)=\xi_0(t)+\frac{(1+f(t))K^{-0.25}-K^{0.25}}{\sqrt{2}(1+f(t))+\sqrt{(1+f(t))}K^{0.25}}+(1+f(t))R_\theta \tag{31}$$

$$C_1(t)=\frac{K^{0.25}}{\sqrt{2(1+f(t))}+K^{0.25}} \tag{32}$$

$$C(t)=\frac{\lambda\chi_0}{(1+f(t))K^{0.5}+\sqrt{0.5+\frac{f(t)}{2}}K^{0.75}} \tag{33}$$

In Eq. (31), $R_\theta=\tan\theta_{sb}/\left(\lambda\chi_0\right)$ is the normalized seabed slope. It should be mentioned that Eqs. (23)–(26), with the use of Eqs. (31)–(33), asymptotically recover the already known solution for the TDP relocation for the static SCR configuration on a horizontal seabed (for that, take $\theta=0$, $f(t)=0$ and $\xi_0(t)=0$, [16]). It also recovers the quasi-static solution for the case of a horizontal and linearly elastic soil, derived in [17], by taking $R_\theta=\tan\theta_{\mathrm{sb}}/\left(\lambda\chi_0\right)=0$. Now, the local non-dimensional dynamic curvature of the riser can be reconstructed from Eq. (15) (for the suspended part) and from Eq. (25) (for the supported part), in the form.

$$\begin{cases}\frac{\chi(\xi,\theta_{\mathrm{sb}},K,t)}{\chi_0}=\frac{1}{1+f(t)}\left(1-\frac{K^{0.25}\exp\left(-\sqrt{1+f(t)}\beta(\xi,\theta_{\mathrm{sb}},t)\right)}{\sqrt{2(1+f(t))}+K^{0.25}}\right); & \beta(\xi,\theta_{\mathrm{sb}},t)>0\\ \frac{\chi(\xi,\theta_{\mathrm{sb}},K,t)}{\chi_0}=\frac{K^{0.5}\exp\left(\frac{K^{0.25}}{\sqrt{2}}\beta(\xi,\theta_{\mathrm{sb}},t)\right)\cos\left(\frac{K^{0.25}}{\sqrt{2}}\beta(\xi,\theta_{\mathrm{sb}},t)\right)}{(1+f(t))K^{0.5}+\sqrt{0.5+\frac{f(t)}{2}}K^{0.75}}; & \beta(\xi,\theta_{\mathrm{sb}},t)<0\end{cases} \tag{34}$$

where

$$\beta\left(\xi,\theta_{\mathrm{sb}},K,t\right)=\xi-\xi_0(t)-\frac{-K^{0.25}+(1+f(t))K^{-0.25}}{\sqrt{2}(1+f(t))+\sqrt{1+f(t)}K^{0.25}}-R_\theta(1+f(t)) \tag{35}$$

Overall, to obtain Eq. (34), for the suspended part in Sect. 2.1, for which, $\beta\left(\xi,\theta_{\mathrm{sb}},t\right)>0$, the governed differential equation on curvature was solved. Then, its derivative (which represents shear for the suspended part) and integrals (first integral leads to the slope diagram, and second integral leads to the elastic deformation) were obtained. It should be mentioned that integrals imply in the appearance of unknown constants, which must be properly defined. For the part of the pipe resting on the seabed in Sect. 2.2, for which $\beta\left(\xi,\theta_{\mathrm{sb}},t\right)<0$, the governed differential equation of the beam (pipe) configuration on elastic seabed was obtained. Then, the first to third derivatives were found (i.e., slope, curvature, shear diagrams). In Sect. 2.3, by matching slope, curvature and shear at the unknown TDP, for both suspended and supported parts, as well continuity, the elastic deformation, slope, curvature, and shear diagrams were obtained. All unknown parameters in Eqs. (31)–(33) were found from a set of the algebraic equations, Eq. (31). Substituting the parameters in every equation for both suspended and resting parts resulted in a continuous configuration, slope, curvature, and shear curve along the structure at TDZ. The verification of the analytical model [e.g., [17]] was conducted by a series of finite element analyses that is discussed in Sect. 3.

Equation (34) shows that the normalized dynamic curvature is a function of the TDP oscillation, $\xi_0(t)$; soil property, K; and slope of the seabed, R_θ. It is worth recalling that the current study is targeted to the assessment of the dynamic curvature and fatigue performance of SCR in TDZ, for different soil stiffness and seabed slopes, the topic that will be discussed in the coming sections.

3 Dynamic curvature of SCR in TDZ

The dynamic curvature of an SCR due to vessel motion is investigated, for a typical and broad range of soil stiffness in the TDZ, by applying the obtained analytical solution. As it should be expected, the effects of both soil stiffness and

TDP oscillation are found as very important factors. Also, a series of finite element analyses were conducted in OrcaFlex® for a typical SCR to verify the analytical results. In the numerical simulations, linear springs were used to model the elastic seabed, and 0.1 m spacing was used between the nodes on the riser in the TDZ. Both ends of the riser at the top connection point and the anchored end were defined as simple hinge boundary conditions. The hydrodynamic coefficients for drag and added mass were considered as 1.2 and 1.0, respectively. Different slopes, including positive slope (which represents NOZ), negative slope (which represents FOZ), and null slope (which represents horizontal and flat seabed), were considered. Seabed slopes of $+2°$ for NOZ and $-1°$ for FOZ were used (see Fig. 5).

The numerical model constructed in OrcaFlex® took a typical SCR, whose main properties are defined in Table 1 [17].

Figure 6 shows the configuration of the numerical model. Two scenarios were considered: first, a small TDP oscillation amplitude, resulting a dynamic tension amplitude of $\tau_0/T_0 = 0.01$; and second, a mild TDP oscillation amplitude, for which $\tau_0/T_0 = 0.03$. The tension oscillations were obtained from the dynamic finite element analysis using OrcaFlex®. The axial rigidity in OrcaFlex® was assumed to be sufficiently high to correlate with the theoretical axial inextensibility implemented in analytical equations.

The TDP oscillation amplitudes ratio (a_0/λ) were observed as 0.27, 0.4, and 0.6 for small oscillations, and 1.2, 1.3, and 1.5 for large oscillations on different seabed slopes (i.e., $-1°$, $0°$, $+2°$), respectively. Both the small and large TDP oscillation amplitudes are of the order of the boundary layer length scale (λ). A critical sector along the SCR, with a length of 2λ and a sharp increase of the curvature, was selected. A total number of 11 nodes were considered with a 0.2λ spacing, where $s/\lambda = -1$ corresponds to the TDP position on the rigid seabed ($\mathrm{Log}K = 8$) (see Fig. 7). The vessel excitation was considered by applying 0.8 m and 1.8 m horizontal surge motion amplitudes, to match identical dynamic tension ratios of $\tau_0/T_0 = 0.01$ (small oscillations) and $\tau_0/T_0 = 0.03$ (mild oscillations) with the analytical results. A sinusoidal motion with period of 15 s was considered, so providing subcritical regime conditions.

Figures 8 and 9 show the non-dimensional results of dynamic curvature oscillation for different seabed slopes, obtained from analytical and numerical analyses, respectively. Without losing generality, the results of curvature dynamics for a mildly rigid ($\mathrm{Log}K = 8$) and soft soil ($\mathrm{Log}K = 2$) were considered as stiffness states. Figure 8 illustrates two entire cycles of non-dimensional analytical results for the dynamic curvature oscillation on FOZ, NOZ, and flat seabed, for small (a–f) and mild (g–l) TDP oscillation amplitudes. It was observed that regardless the soil stiffness, for the nodes near the TDP (node 1),

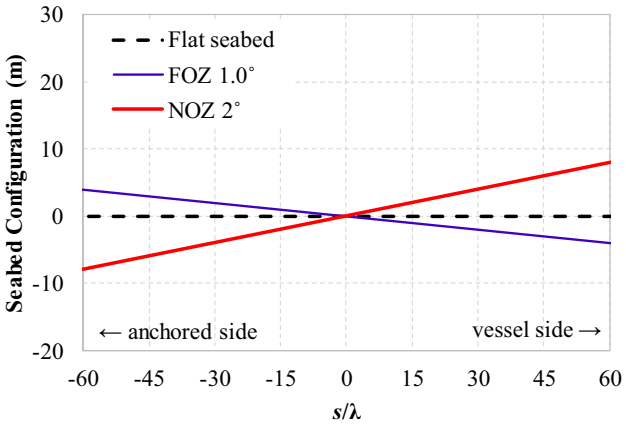

Fig. 5 Considered seabeds, Flat: $\theta_{sb} = 0^{\circ}$, NOZ: $\theta_{sb} = +2^{\circ}$, and FOZ: $\theta_{sb} = -1^{\circ}$

Table 1 Typical SCR data, [17]

Subject	Dimension	Value
Top angle (w.r.t. horiz.)	[deg]	70
Riser length (total)	[m]	5047
Bending stiffness	[Nm^2]	9.915E+06
Axial rigidity*	[N]	2.314E+09
TDP tension	[N]	7.3E+05
External diameter	[m]	0.2032
Depth	[m]	1800
Typical soil modulus	[kN/m/m]	53.3E+02 ($\mathrm{Log}K = 2$)

*Axial rigidity, 2.314E+11 was used in OrcaFlex® modeling, and immersed weight of SCR is 790 N/m

the peak curvature increases in all cases by increasing the TDP oscillation amplitude. The larger TDP oscillation amplitudes cause more nodes on the suspended part to touch the rigid seabed and to experience the null curvature. Also, smoother curvatures were observed on the softer soil seabed.

The analytical sensitivity of each node to the seabed stiffness was then investigated, as shown in Fig. 10 by comparing the non-dimensional values of maximum, minimum, and variation of the curvature. It was observed that increasing the TDP oscillation amplitude causes the maximum curvature (χ_{max}) to increase in the nodes near the seabed. It means that the effect of TDP oscillation amplitude is insignificant in the nodes far away from the seabed (see Fig. 10a, j, d, m, g, and p). Also, this oscillation minimizes the minimum curvature (χ_{min}) for the nodes in TDZ, especially for the nodes far away from the TDP (see Fig. 10b, k, e, d, n, h, and q). The results in Fig. 10 also show that the seabed stiffness variation has a remarkable impact on the minimum curvature (χ_{min}) due to the cyclic contact with the seabed, but

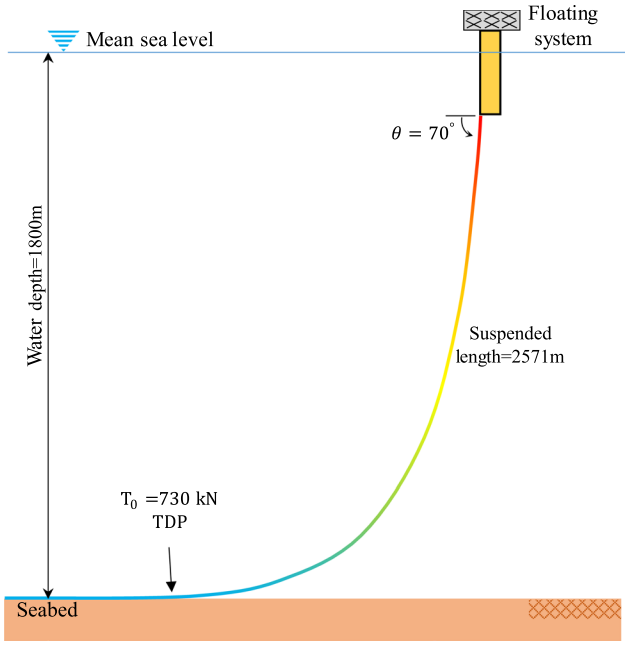

Fig. 6 SCR configuration in numerical simulation

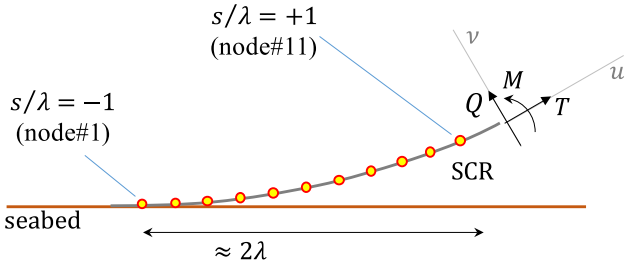

Fig. 7 Schematic view of the critical zone of the SCR

almost no effect on maximum curvatures (χ_{max}). The mild vessel oscillations causes the location of seabed effect on minimum curvature to move toward the vessel (e.g., location $s/\lambda = -0.6$ (node 3) in Fig. 10e for small TDP oscillation amplitude, and $s/\lambda = +2$ (nodes 7) in Fig. 10n for mild TDP oscillation amplitude).

The variation of curvature for each node is defined as the difference between the maximum and minimum curvature, $\Delta\chi$. The nodal changing of dynamic curvature magnitude can be attributed to the combination of the TDP oscillation amplitude effect on the maximum curvature and the soil stiffness effect on the minimum curvature. The magnitude of $\Delta\chi$ is decreased due to the increase in the minimum curvature in the soft soils, and invariant maximum curvature at nodes (see nodes 3 in Fig. 10d–f for small TDP oscillation and node 7 in Fig. 10m–o for large TDP oscillation). Figure 11 shows the curvature variations with different seabed stiffness for both analytical and numerical analyses.

Figure 11 shows that the softer soil provides a smaller amplitude of curvature oscillation in TDZ. The peak coordinates of curvature oscillations in both NOZ and FOZ are in a good agreement, considering the numerical and the analytical results. The maximum curvature has a direct relationship with the TDP oscillation amplitude near the TDP (see maximum curvatures at a few of first nodes in Fig. 11b, e, h, and k). However, this effect is reduced for the nodes far away from TDP [see maximum curvatures at $s/\lambda = 1$ (node 11)]. Also, the soft seabed increases the minimum curvature around the TDP, with no significant effect on nodes far away. This reduces the curvature amplitude (see black lines of curvature variation in Fig. 11b, e, h, and k). In all cases, the peak dynamic curvature is related to seabed stiffness and the TDP oscillation amplitude. The results of numerical and analytical analyses bear a close resemblance in terms of the soil stiffness effect on curvature dynamics in the TDZ.

4 Fatigue response of SCR

A series of simplified fatigue analyses were conducted using vessel motion in surge direction to investigate the effect of seabed soil stiffness in the sloped seabed and its relationship with dynamic curvature oscillation. Recall that the analytical formulation is valid only for subcritical regimes, when the maximum speed of the TDP does not exceed the local transversal wave celerity of a homologous cable. Amplitudes of 1.6 m and 3.2 m in a horizontal direction and a period equal to 15 s was then considered, satisfying the quasi-static motion assumption for the TDP oscillation, so not violating the subcritical regime hypothesis. The DNV E class, SCF = 1.15, $m = 3$, and Log $a = 11.61$, according to DNV-RP-F204 S–N curve, in seawater, was considered. Figure 12 shows the results of the fatigue analysis with the corresponding dynamic curvature oscillation presented in Fig. 13. It was observed that the softer soil results in a greater minimum curvature. Also, the TDP oscillation amplitude in the TDZ has a direct impact on the maximum dynamic curvature as the result of vessel excitation. Increasing the amplitude of oscillation enlarges its magnitude and relocates it toward the vessel.

The fatigue analysis results, on FOZ, NOZ and on flat seabed, show the influence of the TDP motion and soil stiffness. Figure 12 shows that increasing the seabed stiffness and the TDP oscillation amplitude results in increasing the magnitude of damage, regardless the seabed slope.

As concluded in the previous section, by tuning the TDP oscillation amplitude in the analytical investigation, the fatigue life is improved in the FOZ and deteriorated in the NOZ. It means that the trench may have a beneficial or detrimental effect on fatigue life due to different trends of TDP oscillation amplitude on the trench shoulders. This

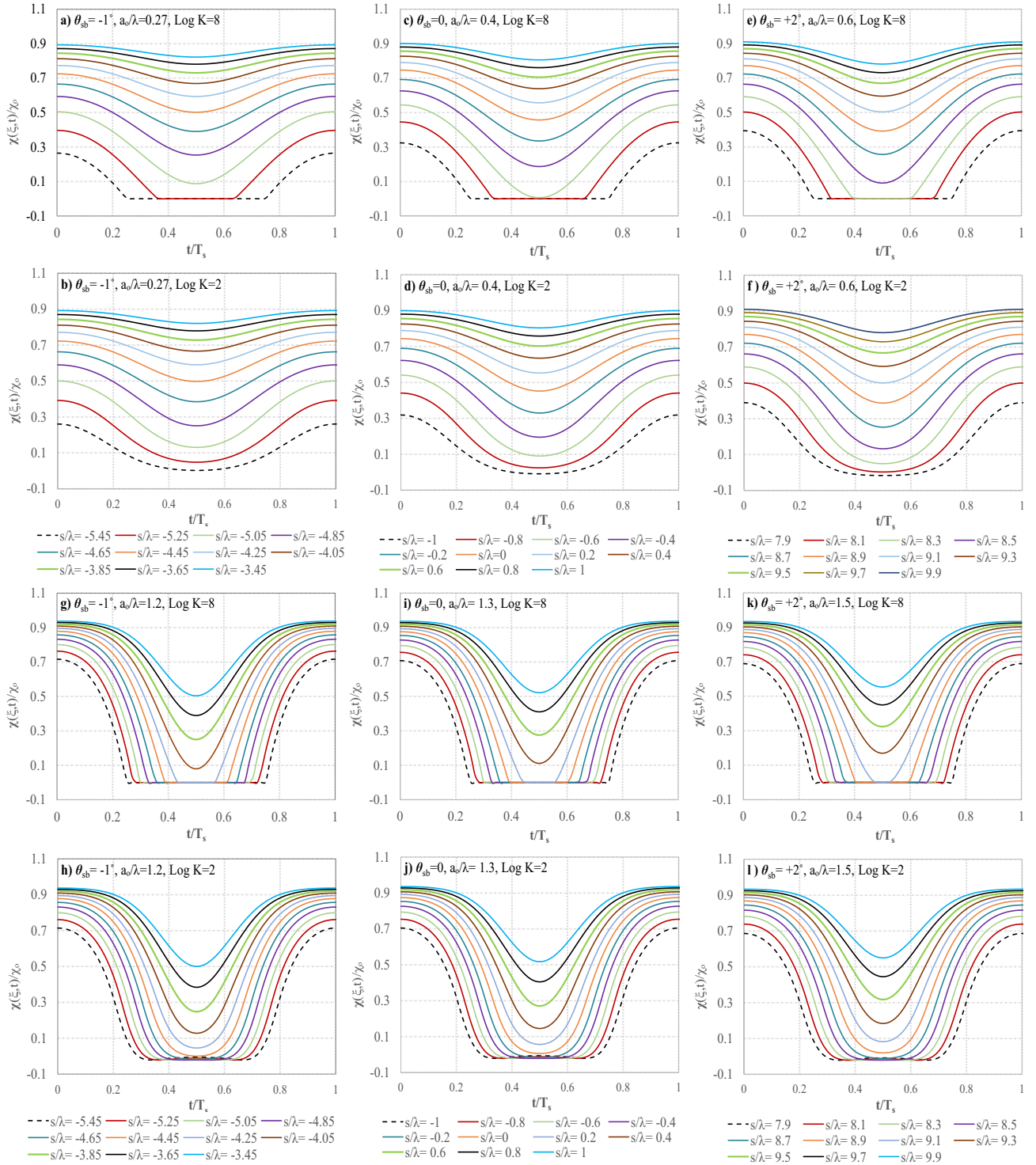

Fig. 8 Non-dimensional dynamic curvature of SCR in TDZ. **a**–**f** analytical solution for small TDP oscillation, $\tau_0/T_0 = 0.01$; **g**–**l** analytical solution for mild TDP oscillation, $\tau_0/T_0 = 0.03$

may justify some of the contradictory predictions found in the literature that have used different environmental loads and seabed properties. The results of numerical fatigue analysis show that there is a close resemblance between the magnitude and the location of the peak dynamic curvature (Fig. 11) and fatigue damage (Fig. 12). The study further revealed the significance of soil stiffness on the minimum

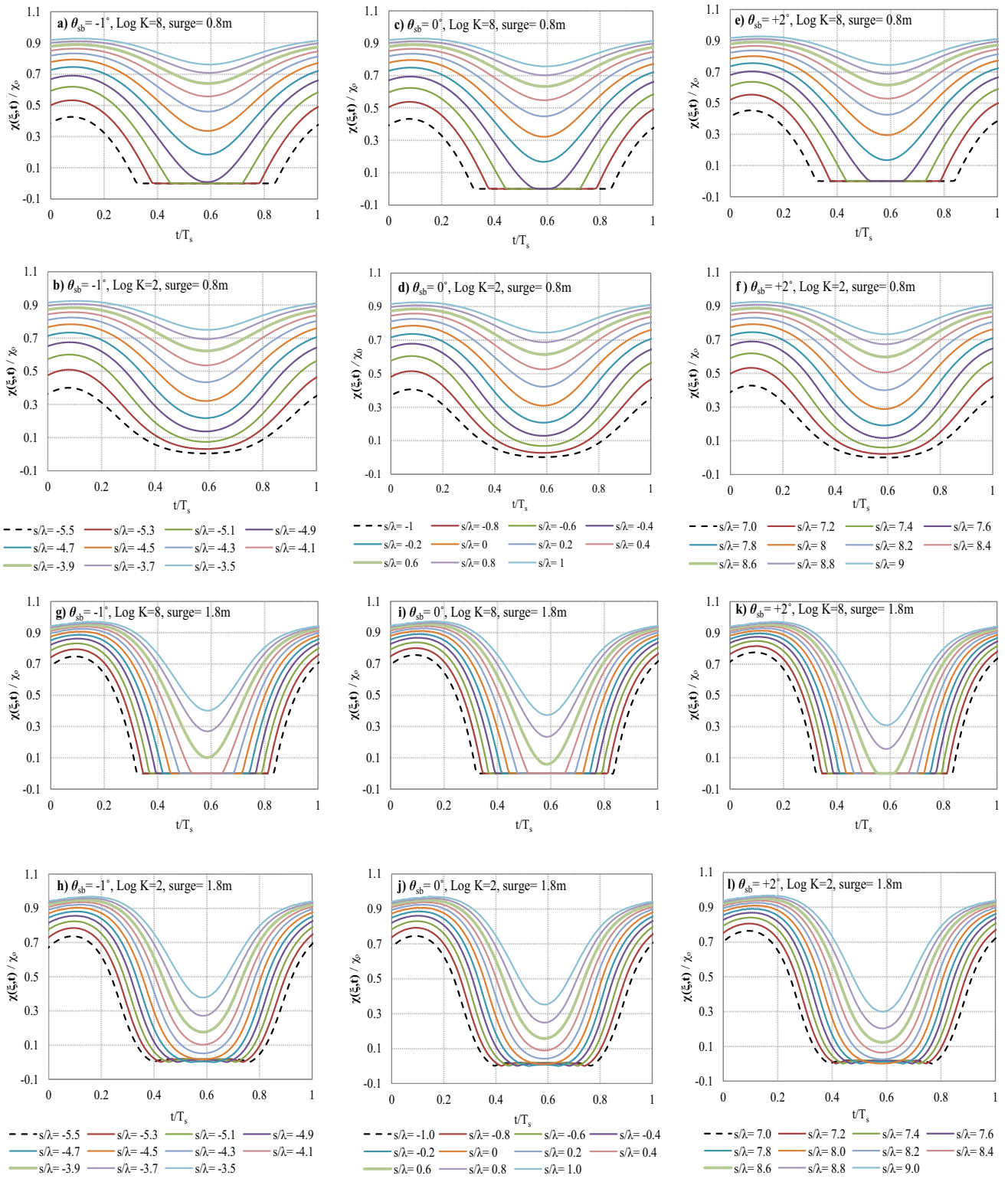

Fig. 9 Non-dimensional dynamic curvature of SCR in TDZ. **a–f** Numerical result for small vessel oscillation, $\tau_0/T_0 = 0.01$; **g–l** numerical result for mild vessel oscillation, $\tau_0/T_0 = 0.03$

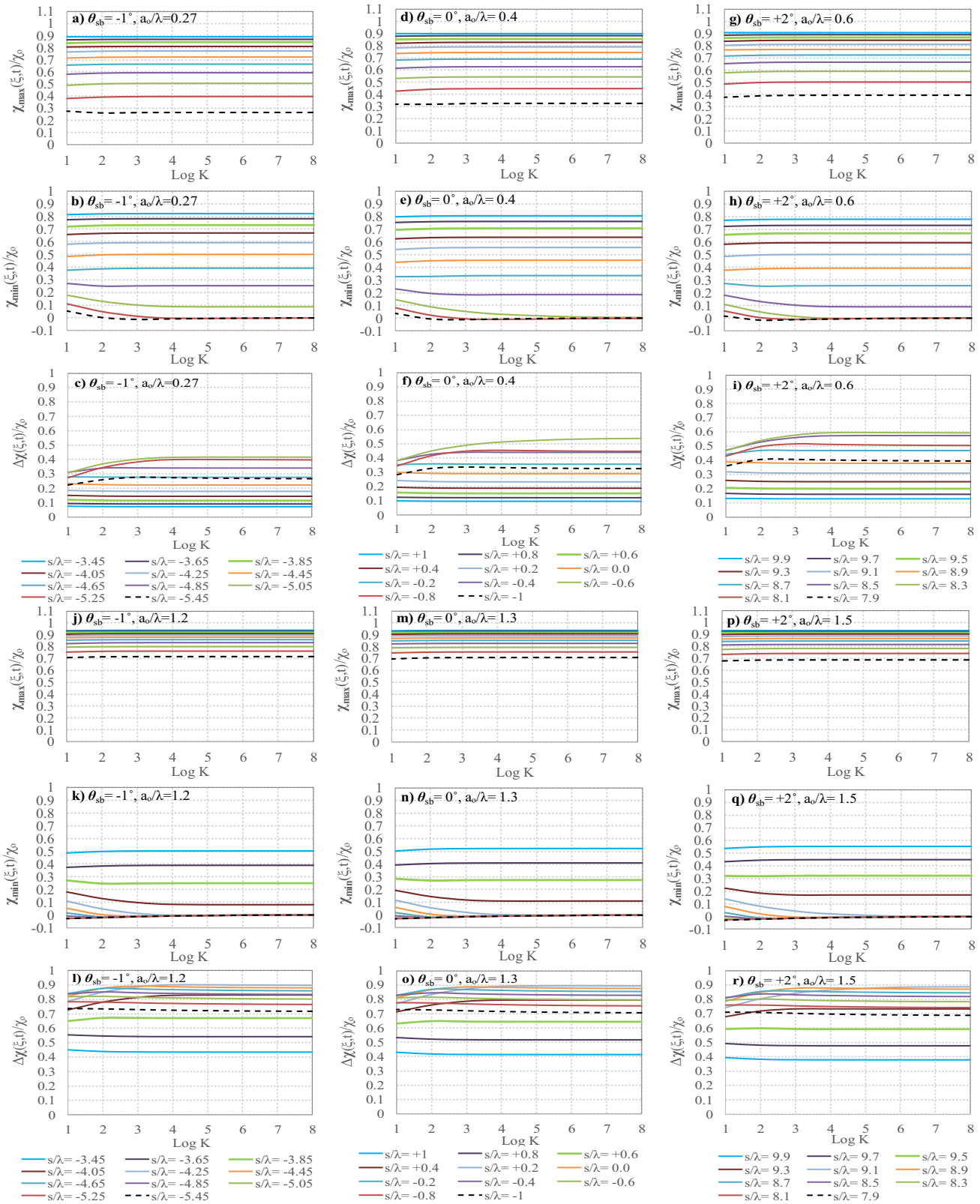

Fig. 10 Nodal curvature sensitivity of SCR to seabed stiffness in TDZ. **a**–**i** analytical solution for small TDP oscillation, $\tau_0/T_0 = 0.01$; **j**–**r** analytical solution for mild TDP oscillation,$\tau_0/T_0 = 0.03$

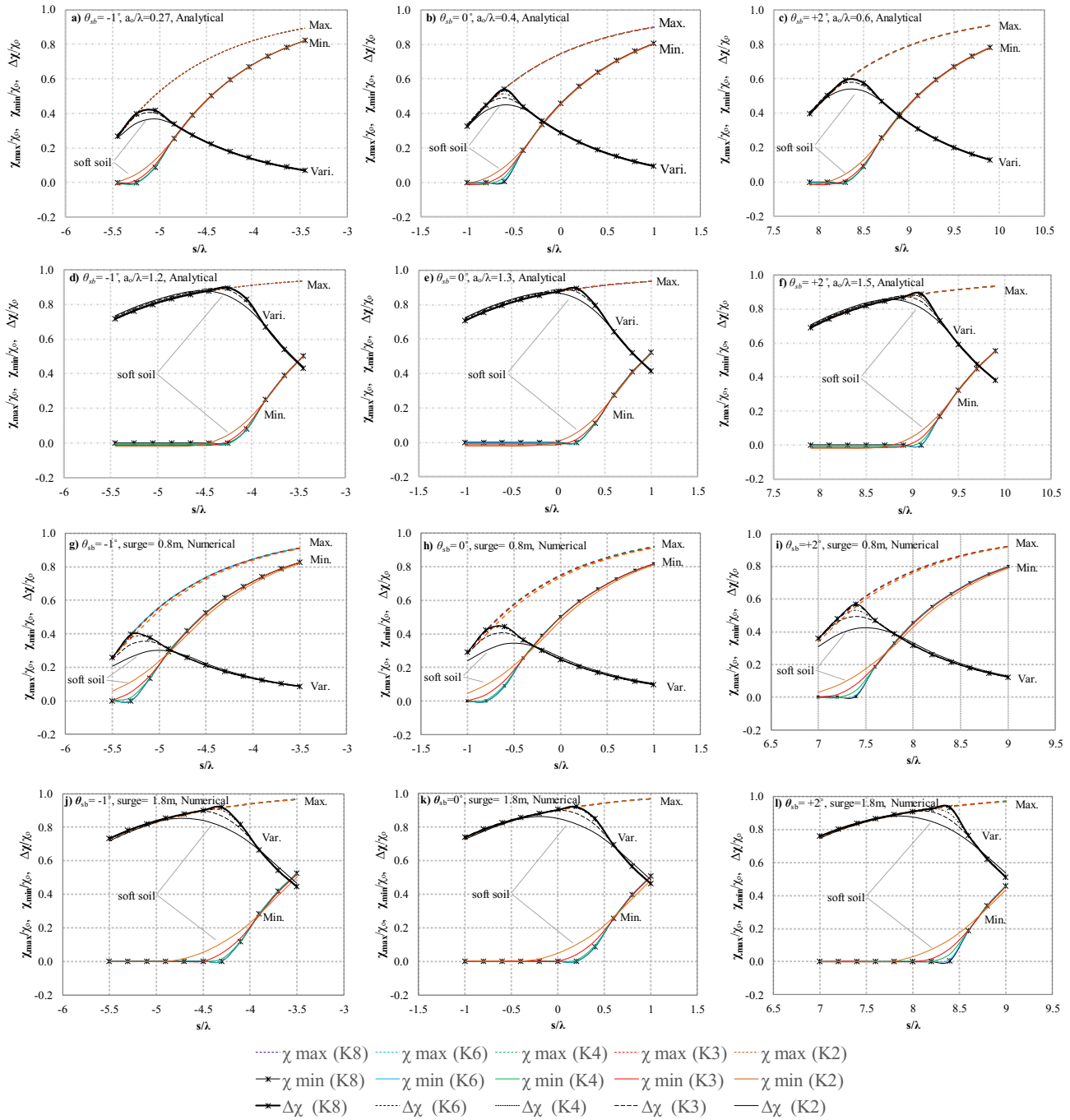

Fig. 11 Non-dimensional dynamic curvature of SCR in TDZ. **a–c** analytical solution for small TDP oscillation, $\tau_0/T_0 = 0.01$; **d–f** analytical solution for mild TDP oscillation, $\tau_0/T_0 = 0.03$; **g–i** numerical result for small vessel oscillation, $\tau_0/T_0 = 0.01$; **j–l** numerical result for mild vessel oscillation, $\tau_0/T_0 = 0.03$

curvature of the riser and the TDP oscillation amplitude that in turn is related to the vessel excitation and trench geometry.

It is worth mentioning that the comparative studies considering the linear elastic and nonlinear hysteretic riser-seabed interactions (e.g., Randolph et al. [4], and Shoghi and Shiri [12, 13]) show that usually the linear elastic seabed yields conservative fatigue lives compared to the nonlinear riser-seabed interaction. Also, the flat seabed results in a conservative fatigue life compared to the trenched seabed for both linear and nonlinear seabed models. Overall, in majority of cases, incorporation of the nonlinear hysteretic riser-seabed interaction models have resulted in reduced

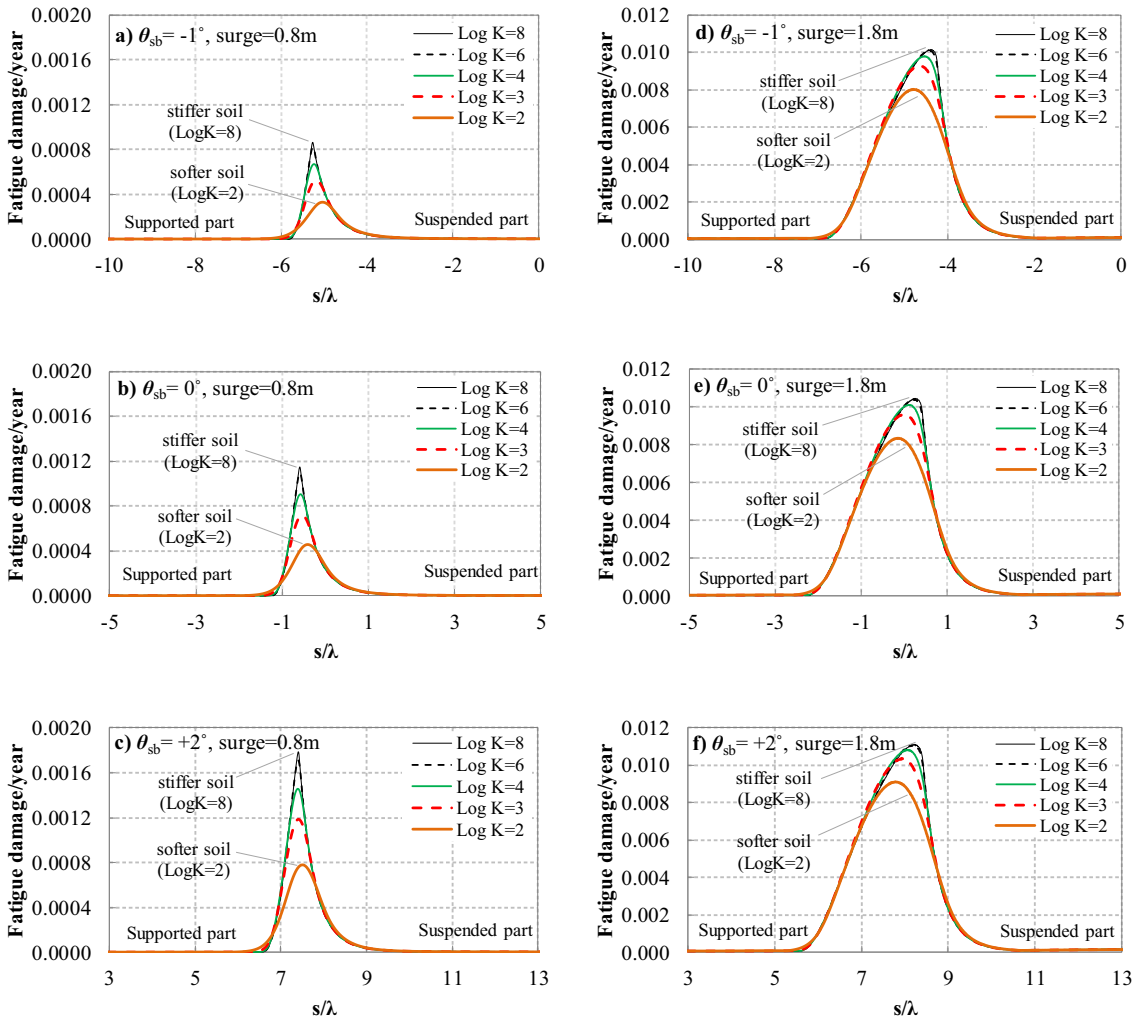

Fig. 12 Fatigue damage distribution on SCR in TDZ. **a–c** result for small vessel oscillation, $\tau_0/T_0 = 0.01$; **d–f** result for mild vessel oscillation, $\tau_0/T_0 = 0.03$

fatigue damage in the TDZ. This fatigue life improvement is particularly pronounced in the NOZ region investigated in the current study. There are several other mechanisms affecting the impact of the riser-seabed interaction on the fatigue life that are currently being explored by researchers such as combined seabed soil remolding and consolidation effects along with riser-seabed-seawater interaction effects (e.g., Janbazi and Shiri [27]).

5 Conclusions

The dynamic curvature oscillation of a typical SCR in TDZ was investigated by deriving a comprehensive analytical model, generalizing a previous one by Pesce et al. [16, 17] by including trench geometry effects considering different seabed slopes. The analytical model was validated by finite element analysis using a commercial software. A range of seabed stiffness was examined, and the corresponding fatigue responses were compared. The study showed that even the effect of the seabed stiffness could be attributed to the geometrical effects of the trench in the TDZ. The study showed that the seabed stiffness has a local effect on SCR and the main contribution of linear soil property (soil stiffness) can be attributed to increasing the local minimum curvature of the SCR, and reducing the dynamic curvature oscillation amplitude. The cyclic range of the curvature was found to be decreased in the TDZ, as the seabed soil becomes softer. In addition, the increase in cyclic tension range might result in a higher fatigue damage accumulation in the TDZ. It was observed that the peak of the accumulated damage curve shifts to the left or right, depending on the slope and stiffness of the seabed soil. The proposed analytical model showed that soil stiffness is always detrimental to fatigue on all slopes and ranges of motion: the more rigid the soil, the greater the accumulated damage. It also showed that a circa

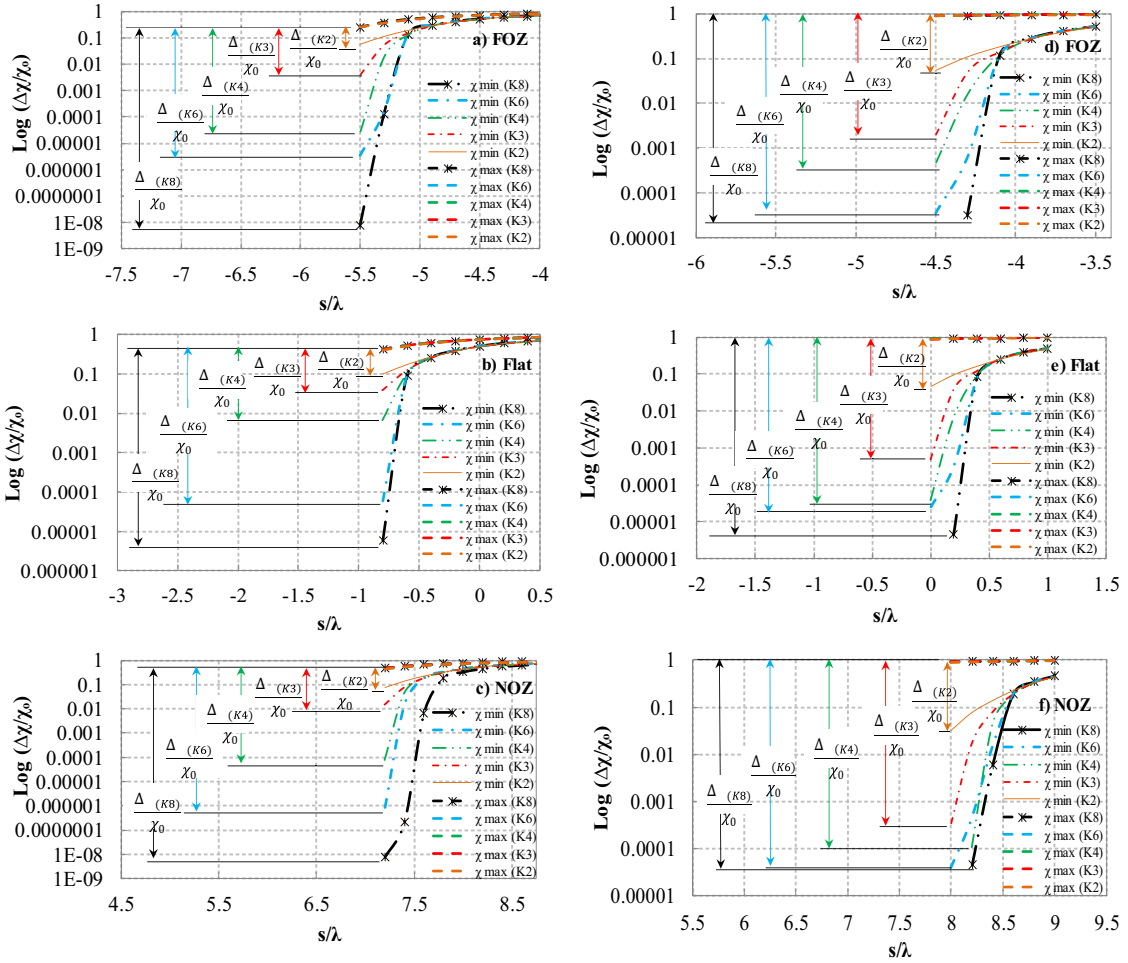

Fig. 13 Non-dimensional dynamic curvature of SCR in TDZ. **a**–**c** result for small vessel oscillation, $\tau_0/T_0 = 0.01$; **d**–**f** result for mild vessel oscillation, $\tau_0/T_0 = 0.03$

twofold increase in the horizontal displacement imposed at the vessel leads to a pronounced increase in the maximum accumulated damage. The increase in ratio between the damage accumulated in the considered situations varies between ~ 12 and ~ 7, if the soil is stiffer, and between about ~ 22 and ~ 11 if the soil is softer, proving that geometry indeed plays a major role in fatigue. Complementarily, it was observed that the accumulated damage peak shifts toward the vessel, as the range of motion increases, causing the riser curve that would join the maximum damage points to bend toward the vessel (analogous to a backbone curve in the dynamic amplitude response of a nonlinear oscillator). The study further supported the idea of the case dependence of the trench effect on fatigue. Depending on the dominant direction of fatigue sea states and low-frequency vessel excursions, the TDP may migrate to FOZ or NOZ of the trench, while oscillating under wave-frequency motions. This, in turn, would result in reduced or increased fatigue life.

All these observations actually bring ascertained facts to be considered in design procedures. For instance, a key factor in selection of the riser wall thickness is fatigue damage. Therefore, different wall thicknesses are used in different zones of the riser with different fatigue damage accumulations. The majority of the published studies show that the fatigue damage is decreased in touchdown point (TDP) by soil softening. This may cause the operators of brown fields and designers of the green fields to feel tranquillity in terms of riser fatigue life because the TDP is used to be known as the most vulnerable point to the fatigue loads. However, the new finding of this paper is mathematically proving that this may not be the case, and extra care should be taken in determination of the wall thicknesses throughout the riser. The damage may be seemed reducing in TDP during the soil softening but indeed the peak damage location is shifted to another part of the riser near the seabed that may have been designed with a wall thickness for a lower fatigue damage. These

new findings become the particular importance in terms of provision of simplified solutions, preferably on the elastic seabed, to incorporate the effect of nonlinear hysteretic riser-seabed interaction and trench formation in fatigue analysis (e.g., Janbazi and Shiri [28]).

Appendix. Dynamic equilibrium equations for the planar problem of a catenary riser

This Appendix brings a derivation that can be found in a more detailed analysis in Pesce [15], Chapter 4, Section 4.1. It is however essential for the understanding of the local analysis close to TDP, carried out through the boundary layer technique, in the main core of the text. Consider a planar problem of a riser suspended from a floating unity, whose static configuration is characterized by the functions $\theta(s)$, $T(s)$ and $Q(s)$, respectively, the angle of the line with respect to the horizontal, the effective tension and the shear force at a given section s. Let their dynamic counterparts be written as,

$$\begin{aligned}\Theta(s,t) &= \theta(s) + \gamma(s,t)\\ T(s,t) &= T(s) + \tau(s,t)\\ Q(s,t) &= Q(s) + \vartheta(s,t)\end{aligned} \tag{36}$$

where $\gamma(s,t)$, $\tau(s,t)$ and $\vartheta(s,t)$ are the corresponding perturbed values, resulting from dynamic loads acting on the riser in the vertical plane. Let also $u(s,t)$ and $v(s,t)$ be small displacements around the static equilibrium configuration in their tangential and normal directions, respectively. To first order, the following well-known kinematic relation can be promptly derived (Fig. 14).

$$\gamma(s,t) = \frac{\partial v}{\partial s} + u\frac{\mathrm{d}\theta}{\mathrm{d}s} \tag{37}$$

Taking a small segment Δs, the resultant of effective tension and shear force projected onto the tangential and normal directions of the static configuration is readily obtained in the form:

$$\begin{aligned}\Delta F_u &= T(s+\Delta s,t)\cos\left(\Delta\theta + \gamma(s+\Delta s,t)\right) - T(s,t)\cos\gamma(s,t)\\ &\quad - \left(Q(s+\Delta s,t)\sin\left(\Delta\theta + \gamma(s+\Delta s,t)\right) - Q(s)\sin\gamma(s,t)\right)\\ \Delta F_v &= Q(s+\Delta s,t)\cos\left(\Delta\theta + \gamma(s+\Delta s,t)\right) - Q(s)\cos\gamma(s,t)\\ &\quad + \left(T(s+\Delta s,t)\sin\left(\Delta\theta + \gamma(s+\Delta s,t)\right) - T(s,t)\sin\gamma(s,t)\right)\end{aligned} \tag{38}$$

If only first-order terms in $\Delta\theta$ and γ are retained, Eq. (38) reduces to

$$\begin{aligned}\Delta F_u &\cong T(s+\Delta s,t) - T(s,t) - \left(Q(s+\Delta s,t)\Delta\theta\right.\\ &\quad \left. + Q(s+\Delta s,t)\gamma(s+\Delta s,t) - Q(s)\gamma(s,t)\right)\\ \Delta F_v &\cong Q(s+\Delta s,t) - Q(s) + \left(T(s+\Delta s,t)\Delta\theta\right.\\ &\quad \left. + T(s+\Delta s,t)\gamma(s+\Delta s,t) - T(s,t)\gamma(s,t)\right)\end{aligned} \tag{39}$$

The dynamic equilibrium equation of the segment Δs then reads

$$\begin{aligned}\Delta F_u + h_u\Delta s - q\sin\theta\Delta s &= m\frac{\partial^2 u}{\partial t^2}\Delta s\\ \Delta F_v + h_v\Delta s - q\cos\theta\Delta s &= m\frac{\partial^2 v}{\partial t^2}\Delta s\end{aligned} \tag{40}$$

where

$$\begin{aligned}h_u(s,t) &= h_u(s) + \varpi_u(s,t)\\ h_v(s,t) &= h_v(s) + \varpi_v(s,t)\end{aligned} \tag{41}$$

refer to the hydrodynamic forces, q is the immersed weight, and m is the mass of the structure, all per unit length. The

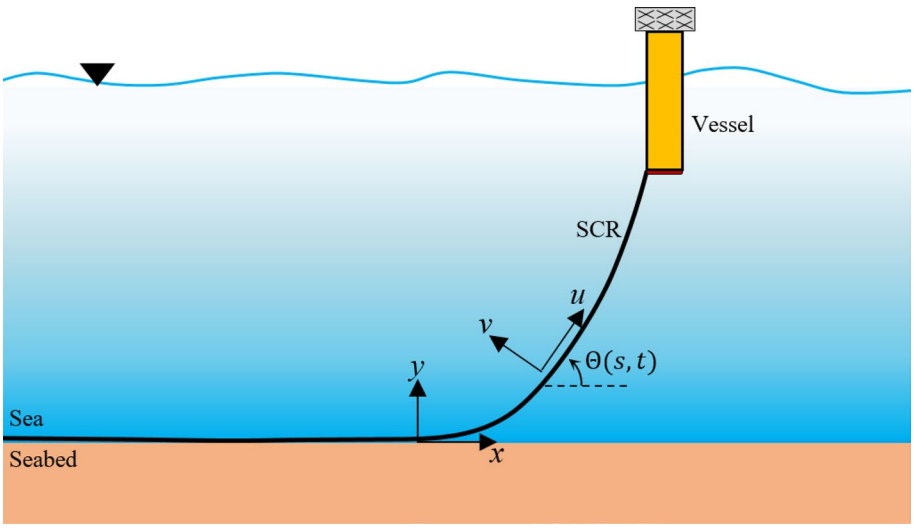

Fig. 14 Schematic view of planar problem

terms $h_{u,v}(s)$ and $\varpi_{u,v}(s,t)$ are the components of the static and dynamic parcels of the hydrodynamic force in the tangential and normal direction, regarding the static configuration. The last ones are due to the relative external water flow with respect to the riser, at section s, usually modeled through the well-known Morison's formula. Equations (40) transform into partial differential ones, by the usual process of taking the limit when $\Delta s \to 0$, in the following form:

$$\begin{aligned}&\frac{\partial T}{\partial s} - (T\gamma + Q)\frac{\mathrm{d}\theta}{\mathrm{d}s} - \frac{\partial}{\partial s}(Q\gamma) + h_u + \varpi_u - q\sin\theta = m\frac{\partial^2 u}{\partial t^2}\\ &\frac{\partial Q}{\partial s} + (T - Q\gamma)\frac{\mathrm{d}\theta}{\mathrm{d}s} + \frac{\partial}{\partial s}(T\gamma) + h_v + \varpi_v - q\cos\theta = m\frac{\partial^2 v}{\partial t^2}\end{aligned} \tag{42}$$

Alternatively, Eq. (42) may be written with the use of the kinematic relation (37) as,

$$\begin{aligned}&\frac{\partial T}{\partial s} - \left[T\left(\frac{\partial v}{\partial s} + u\frac{\mathrm{d}\theta}{\mathrm{d}s}\right) + Q\right]\frac{\mathrm{d}\theta}{\mathrm{d}s} - \frac{\partial}{\partial s}\left[Q\left(\frac{\partial v}{\partial s} + u\frac{\mathrm{d}\theta}{\mathrm{d}s}\right)\right]\\ &+ h_u + \varpi_u - q\sin\theta = m\frac{\partial^2 u}{\partial t^2}\\ &\frac{\partial Q}{\partial s} + \left[T - Q\left(\frac{\partial v}{\partial s} + u\frac{\mathrm{d}\theta}{\mathrm{d}s}\right)\right]\frac{\mathrm{d}\theta}{\mathrm{d}s} + \frac{\partial}{\partial s}\left[T\left(\frac{\partial v}{\partial s} + u\frac{\mathrm{d}\theta}{\mathrm{d}s}\right)\right]\\ &+ h_v + \varpi_v - q\cos\theta = m\frac{\partial^2 v}{\partial t^2}\end{aligned} \tag{43}$$

Notice that by using Eqs. (36b,c), (42) may be also rewritten as,

$$\begin{aligned}&\left\{\frac{\partial T}{\partial s} - Q\frac{\mathrm{d}\theta}{\mathrm{d}s} + h_u - q\sin\theta\right\}\\ &+ \left\{\frac{\partial \tau}{\partial s} - (T\gamma + \vartheta)\frac{\mathrm{d}\theta}{\mathrm{d}s} - \frac{\partial}{\partial s}(Q\gamma) + \varpi_u\right\} = m\frac{\partial^2 u}{\partial t^2}\\ &\left\{\frac{\partial Q}{\partial s} + T\frac{\mathrm{d}\theta}{\mathrm{d}s} + h_v - q\cos\theta\right\}\\ &+ \left\{\frac{\partial \vartheta}{\partial s} + (\tau - Q\gamma)\frac{\mathrm{d}\theta}{\mathrm{d}s} + \frac{\partial}{\partial s}(T\gamma) + \varpi_v\right\} = m\frac{\partial^2 v}{\partial t^2}\end{aligned} \tag{44}$$

or, from (43),

$$\begin{aligned}&\left\{\frac{\partial T}{\partial s} - Q\frac{\mathrm{d}\theta}{\mathrm{d}s} + h_u - q\sin\theta\right\} + \left\{\frac{\partial \tau}{\partial s} - \left(T\left(\frac{\partial v}{\partial s} + u\frac{\mathrm{d}\theta}{\mathrm{d}s}\right) + \vartheta\right)\frac{\mathrm{d}\theta}{\mathrm{d}s}\right.\\ &\left. - \frac{\partial}{\partial s}\left(Q\left(\frac{\partial v}{\partial s} + u\frac{\mathrm{d}\theta}{\mathrm{d}s}\right)\right) + \varpi_u\right\} = m\frac{\partial^2 u}{\partial t^2}\\ &\left\{\frac{\partial Q}{\partial s} + T\frac{\mathrm{d}\theta}{\mathrm{d}s} + h_v - q\cos\theta\right\} + \left\{\frac{\partial \vartheta}{\partial s} + \left(\tau - Q\left(\frac{\partial v}{\partial s} + u\frac{\mathrm{d}\theta}{\mathrm{d}s}\right)\right)\frac{\mathrm{d}\theta}{\mathrm{d}s}\right.\\ &\left. + \frac{\partial}{\partial s}\left(T\left(\frac{\partial v}{\partial s} + u\frac{\mathrm{d}\theta}{\mathrm{d}s}\right)\right) + \varpi_v\right\} = m\frac{\partial^2 v}{\partial t^2}\end{aligned} \tag{45}$$

The first terms in brackets, either in Eqs. (44) or (45) are, in fact, Love's equations for the static equilibrium of curved bars on the plane. Therefore, they are identically null. The (perturbed) dynamic variables are, therefore, governed by the following coupled nonlinear partial differential equations:

$$\begin{aligned}&\frac{\partial \tau}{\partial s} - ((T + \tau)\gamma + \vartheta)\frac{\mathrm{d}\theta}{\mathrm{d}s} - \frac{\partial}{\partial s}((Q + \vartheta)\gamma) + \varpi_u = m\frac{\partial^2 u}{\partial t^2}\\ &\frac{\partial \vartheta}{\partial s} + (\tau - (Q + \vartheta)\gamma)\frac{\mathrm{d}\theta}{\mathrm{d}s} + \frac{\partial}{\partial s}((T + \tau)\gamma) + \varpi_v = m\frac{\partial^2 v}{\partial t^2}\end{aligned} \tag{46}$$

or, given just in terms of the displacements $u(s,t)$ and $v(s,t)$,

$$\begin{aligned}&\frac{\partial \tau}{\partial s} - \left((T + \tau)\left(\frac{\partial v}{\partial s} + u\frac{\mathrm{d}\theta}{\mathrm{d}s}\right) + \vartheta\right)\frac{\mathrm{d}\theta}{\mathrm{d}s}\\ &- \frac{\partial}{\partial s}\left((Q + \vartheta)\left(\frac{\partial v}{\partial s} + u\frac{\mathrm{d}\theta}{\mathrm{d}s}\right)\right) + \varpi_u = m\frac{\partial^2 u}{\partial t^2}\\ &\frac{\partial \vartheta}{\partial s} + \left(\tau - (Q + \vartheta)\left(\frac{\partial v}{\partial s} + u\frac{\mathrm{d}\theta}{\mathrm{d}s}\right)\right)\frac{\mathrm{d}\theta}{\mathrm{d}s}\\ &+ \frac{\partial}{\partial s}\left((T + \tau)\left(\frac{\partial v}{\partial s} + u\frac{\mathrm{d}\theta}{\mathrm{d}s}\right)\right) + \varpi_v = m\frac{\partial^2 v}{\partial t^2}\end{aligned} \tag{47}$$

On the other hand, the third planar static Love's equation that relates bending moment and shear force may be written, in the absence of any external applied moment per unit length as,

$$\frac{\partial M}{\partial s} + Q = 0 \tag{48}$$

Consistently with the kinematic relation (37), and considering that the slenderness of the structure makes the effect of the rotatory inertia negligible, the corresponding dynamic equation regarding the rotation would be written as:

$$\frac{\partial \mu}{\partial s} + \vartheta = 0 \tag{49}$$

where $\mu(s,t)$ is the dynamic parcel of the bending moment. In fact, this is a quasi-static approximation.

Therefore, bending moment and shear may be said to be simply related by

$$\frac{\partial M}{\partial s} + Q = 0 \tag{50}$$

On the other hand, from the three basic and usual hypotheses: (1) small strains; (2) linear relations between stresses and strains; (3) Kirchhoff's 'plane sections remain plane after deformation,' the following constitutive equation may be assumed valid:

$$M(s,t) = EI\frac{\partial \Theta}{\partial s} = EI\chi(s,t) \tag{51}$$

where EI is the bending stiffness at section s, and $\chi(s,t)$ is the total curvature. The following relations, regarding the static and dynamic parcels, are then promptly derived:

$$\begin{aligned}&M(s) = EI\frac{\mathrm{d}\theta}{\mathrm{d}s}\\ &\mu(s,t) = EI\frac{\partial \gamma}{\partial s} \cong EI\left[\frac{\partial^2 v}{\partial s^2} + \frac{\partial}{\partial s}\left(u\frac{\mathrm{d}\theta}{\mathrm{d}s}\right)\right]\end{aligned} \tag{52}$$

From (48) and (49), it follows that

$$\begin{aligned} Q(s) &= -\frac{\partial}{\partial s}\left(EI\frac{\mathrm{d}\theta}{\mathrm{d}s}\right) \\ \vartheta(s,t) &= -\frac{\partial}{\partial s}\left(EI\frac{\partial^2 v}{\partial s^2} + EI\frac{\partial}{\partial s}\left(u\frac{\mathrm{d}\theta}{\mathrm{d}s}\right)\right) \end{aligned} \tag{53}$$

Also, using (51) in (50) and then substituting the result in Eq. (42,b), it follows that

$$-\frac{\partial^2}{\partial s^2}(EI\chi) + \left(\mathrm{T} - \frac{\partial}{\partial s}(EI\chi)\gamma\right)\frac{d\theta}{ds} + \frac{\partial}{\partial s}(\mathrm{T}\gamma) + h_v + \varpi_v - q\cos\theta = m\frac{\partial^2 v}{\partial t^2} \tag{54}$$

In the common case in which the bending stiffness is assumed constant along the line, Eq. (54) reduces to:

$$-EI\frac{\partial^2\chi}{\partial s^2} - \gamma EI\frac{\mathrm{d}\theta}{\mathrm{d}s}\frac{\partial\chi}{\partial s} + T\chi + \gamma\frac{\partial T}{\partial s} + h_v + \varpi_v - q\cos\theta = m\frac{\partial^2 v}{\partial t^2} \tag{55}$$

Equation (55) is a fundamental result to be used in the local analysis, close to TDP, via the boundary layer technique. It can be used in the vicinity of the hang-off point as well, see [15].

Acknowledgements The authors gratefully acknowledge the financial support of this research by the Research and Development Corporation (RDC) (now Innovate NL) through the Ignite funding program, the "Natural Science and Engineering Research Council of Canada (NSERC)" through Discovery program, and the Memorial University of Newfoundland through VP start-up funding support. The third author acknowledges a research grant from CNPq, the Brazilian National Council for Scientific Research, process 308230/2018-3 and the financial support by CAPES, the Coordination for the Improvement of Higher Education Personnel (CAPES) in Brazil, through the International Exchange Program PRInt-USP/2019.

References

1. Bridge CD, Howells HA (2007) Observation and modeling of steel catenary riser trenches. In: Proceedings of the 17th international society of offshore and polar engineers conference. ISOPE-I-07-321, Lisbon
2. Langner C (2003) Fatigue life improvement of steel catenary risers due to self- trenching at the touchdown point. In: Offshore technology conference. OTC-15104-MS, Texas. https://doi.org/10.4043/15104-MS
3. Wang K, Low YM (2016) Study of seabed trench induced by steel catenary riser and seabed interaction. In: Proceedings of the 35th international conference on ocean, offshore and arctic engineering. OMAE2016-54236, Busan. https://doi.org/10.1115/OMAE2016-54236
4. Randolph MF, Bhat S, Jain S. Mekha B (2013) Modeling the touchdown zone trench and its impact on SCR fatigue life. In: Proceedings of the offshore technology conference; OTC-23975-MS, Houston. https://doi.org/10.4043/23975-MS
5. Shiri H (2014) Response of steel catenary risers on hysteretic non-linear seabed. Appl Ocean Res 44:20–28. https://doi.org/10.1016/j.apor.2013.10.006
6. Shiri H (2014) Influence of seabed trench formation on fatigue performance of steel catenary risers in touchdown zone. Mar Struct 36:1–20. https://doi.org/10.1016/j.marstruc.2013.12.003
7. Shiri H, Randolph MF (2010) Influence of seabed response on fatigue performance of steel catenary risers in touchdown zone. In: Proceeding of the 29th international conference on ocean, offshore and arctic engineering; OMAE2010-20051, Shanghai
8. Campbell M (1999) The complexities of fatigue analysis for deepwater risers. In: Proceedings of the deepwater pipeline conference, New Orleans, USA
9. Aubeny C, Biscontin G (2008) Interaction model for steel compliant riser on soft seabed. In: Offshore technology conference. OTC-19493-MS, Houston
10. Aubeny C, Biscontin G (2009) Seafloor-riser interaction model. Int J Geomech 9(3):133–141. https://doi.org/10.1061/(ASCE)1532-3641(2009)9:3(133)
11. Clukey EC, Young AG, Dobias JR, Garmon GR (2008) Soil response and stiffness laboratory measurements of SCR pipe/soil interaction. In: Offshore technology conference; OTC-19303-MS, Houston. https://doi.org/10.4043/19303-MS
12. Shoghi R, Shiri H (2019) Modelling touchdown point oscillation and its relationship with fatigue response of steel catenary risers. Appl Ocean Res 87:142–154. https://doi.org/10.1016/j.apor.2019.03.010
13. Shoghi R, Shiri H (2020) Re-assessment of trench effect on fatigue performance of steel catenary risers in the touchdown zone. Appl Ocean Res 94:1–16. https://doi.org/10.1016/j.apor.2019.101989
14. Aranha JAP, Martins CA, Pesce CP (1997) Analytical approximation for the dynamic bending moment at the touchdown point of a catenary riser. Int J Offshore Polar Eng 7(4):241–249
15. Pesce CP (1997) Mechanics of cables and tubes in catenary configuration: an analytical and experimental approach. ['Livre-Docência' Thesis, in Portuguese]. University of São Paulo
16. Pesce CP, Aranha JAP, Martins CA (1998) The soil rigidity effect in the touchdown boundary layer of a catenary riser: static problem. In: Proceedings of the 8th international offshore and polar engineering conference. ISOPE-I-98-130, Montreal
17. Pesce CP, Martins CA, Silveira LM (2006) Riser–soil interaction: local dynamics at TDP and a discussion on the eigenvalue and the VIV problems. J Offshore Mech Arct Eng 128(1):39–55. https://doi.org/10.1115/1.2151205
18. Randolph MF, Quiggin P (2009) Non-linear hysteretic seabed model for catenary pipeline contact. In: Proceedings of the 28th international conference on ocean, offshore and arctic engineering OMAE 2009-79259. Hawaii, USA
19. Shoghi R, Pesce CP, Shiri H (2021) Influence of trench geometry on fatigue response of steel catenary risers by using a boundary layer solution on a sloped seabed. Ocean Eng 221:108447. https://doi.org/10.1016/j.oceaneng.2020.108447
20. Triantafyllou MS, Triantafyllou GS (1991) The paradox of the hanging string an: explanation using singular perturbation. J Sound Vib 148(2):343–351. https://doi.org/10.1016/0022-460X(91)90581-4
21. Burgess JJ (1992) Bending stiffness in a simulation of undersea cable deployment. Int J Offshore Polar Eng 3(3):197–204
22. Dhotarad MS, Ganesan N, Rao BVA (1978) Transmission line vibration with 4R dampers. J Sound Vib 60(4):604–606. https://doi.org/10.1016/S0022-460X(78)80101-1
23. Irvine M (1993) Local bending stresses in cables. Int J Offshore Polar Eng 3(3):172–175
24. Pesce CP, Pinto MMO (1996) First-order dynamic variation of curvature and tension in catenary risers. In: The 6th international offshore and polar engineering conference. ISOPE-I-96-107, Los Angeles
25. Pesce CP, Aranha JAP, Martins CA, Ricardo OGS, Silva S (1997) Dynamic curvature in catenary risers at the touch down point: an

experimental study and the analytical boundary layer solution. In: Proceedings of the 17th international offshore and polar engineering conference, Honolulu, vol 2, pp 656–665
26. Love AEH (1927) A treatise on the mathematical theory of elasticity, 4th edn. Dover Publications, New York
27. Janbazi H, Shiri H (2023) Investigation of trench effect on fatigue response of steel catenary risers using an effective stress analysis. Comput Geotech 160:105506. https://doi.org/10.1016/j.compgeo.2023.105506
28. Janbazi H, Shiri H (2023) A hybrid model to simulate the trench effect on the fatigue analysis of steel catenary risers in the touchdown zone. Can Geotech J. https://doi.org/10.1139/cgj-2022-0103